Free Volume, Adhesion, and Viscoelastic Properties of Model Nanostructured Pressure-Sensitive Adhesive Based on Stoichiometric Complex of Poly(*N*-vinyl pyrrolidone) and Poly(ethylene glycol) of Disparate Chain Lengths

Mikhail M. Feldstein,[1] Eugenia V. Bermesheva,[1] Y. C. Jean,[2] Gauri P. Misra,[3,4] Ronald A. Siegel[3,4]

[1]*A.V. Topchiev Institute of Petrochemical Synthesis, Russian Academy of Sciences, 119991 Moscow, Russia*
[2]*Department of Chemistry, University of Missouri—Kansas City (UMKC), Kansas City, Missouri 64110-2399*
[3]*Department of Pharmaceutics, University of Minnesota, Minneapolis, Minnesota 55455*
[4]*Department of Biomedical Engineering, University of Minnesota, Minneapolis, Minnesota 55455*

Received 26 April 2010; accepted 6 June 2010
DOI 10.1002/app.32917
Published online 1 September 2010 in Wiley Online Library (wileyonlinelibrary.com).

ABSTRACT: Positron annihilation lifetime spectroscopy was used to characterize the size and content of subnanoscopic free volume in a model pressure-sensitive adhesive based on a stoichiometric hydrogen-bonded network complex of poly(*N*-vinyl pyrrolidone) (PVP) and oligomeric poly(ethylene glycol) (PEG). Adhesive properties were examined with peel and probe tack tests, and mechanical properties were studied with tensile test. Nonequimolar stoichiometry and the structure of PVP–PEG model pressure-sensitive adhesive blends were found to be determined by the length of PEG short chains. The size and number density of free volume domains in the PVP–PEG blends were determined as functions of blend composition and relative humidity of the surrounding atmosphere, which controls the amount of absorbed water. Correlating the free volume, adhesion behaviors, and tensile properties of the blends, the range of free volume favoring pressure-sensitive adhesion in examined compositions was established. © 2010 Wiley Periodicals, Inc. J Appl Polym Sci 119: 2408–2421, 2011

Key words: adhesion; mechanical properties; networks; self-assembly; structure-property relations

INTRODUCTION

The mobility of particles in a closely packed material primarily depends on the degree of packing, or free volume of the material. The free volume of a material is defined as the difference between the bulk volume and the sum of the hard core and vibrational volumes of the constituent building blocks. Thus, the free volume of a polymer is the unoccupied space, or vacancies, available for segmental motion. Free volume concepts have long been used to interpret and explain the glass transition[1–3] and glass transition temperature,[4–8] viscoelastic[2,5,9–11] and relaxation[9,12–14] behaviors, diffusion, and other transport properties of polymer systems.[7,15–23] Along with the energy of intermolecular cohesion, free volume is a factor controlling the values of cohesive energy density, solubility parameter,[24] and the Flory–Huggins interaction parameter.[25]

Polymer adhesion is a complex phenomenon, including contributions of adsorption, diffusion, and viscoelastic deformation processes.[26–28] From this standpoint, it is reasonable to expect that free volume affects the adhesive behavior of polymers. However, measurement of free volume in adhesive polymers has been the subject of only few research papers,[29–31] and no attempts have been made, to our knowledge, to compare adhesion and free-volume behaviors.

Pressure-sensitive adhesives (PSAs) are a special class of viscoelastic polymers that form strong adhesive joints with substrates of various chemical nature under application of slight external pressures (1–10 Pa) over short periods of time (1–5 s).[32] To be a PSA, a polymer should possess both high fluidity under applied bonding pressure, to form good adhesive contact, and high-cohesive strength, and elasticity, which are necessary for resistance to debonding stresses and for dissipation of mechanical energy at the stage of adhesive bond failure under detaching force. These conflicting properties are difficult to combine in a single polymer material.

As was recently shown,[33] the strength of PSA adhesive joints is controlled by a combination of diffusion, viscoelastic, and relaxation mechanisms. At the molecular level, strong adhesion is the result of a narrow balance between high-cohesive strength and

Correspondence to: M. M. Feldstein (mfeld@ips.ac.ru).

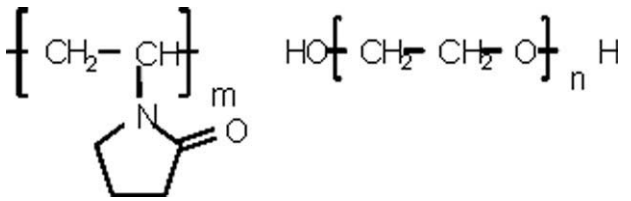

Figure 1 Chemical structures of high molecular weight PVP (left) and PEG oligomers (right). $m \approx 10{,}000$ and $n = 5$–15.

large free volume.[33] Individually, high-cohesive interaction energy and large free volume are necessary but insufficient prerequisites for PSA strength. Measurement of free volume in PSA polymer composites was the objective of a previous report.[34] In this study, free-volume size, distribution, and content were evaluated by positron annihilation lifetime spectroscopy (PALS), as functions of the type of intermolecular bonds and the depth profile for a model PSA based on a hydrogen bonded complex of high molecular weight poly(*N*-vinyl pyrrolidone) (PVP) with poly(ethylene glycol) (PEG) oligomer of molecular weight 400 g/mol. Neither PVP nor PEG is individually adhesive, but strongly adhesive blends are found over a very narrow range of PVP–PEG composition, which is affected by relative humidity (RH).[35,36] This behavior makes the PVP–PEG–H_2O system a convenient model to gain insight into molecular structures featured in PSAs.[33,37]

Complete miscibility in the PVP–PEG system has been studied using wedge micro-interferometry, which measures concentration profiles and interdiffusion coefficients.[38,39] Although short-chain PEG fractions of M_w 200–600 g/mol are miscible with PVP, higher molecular weight PEG fractions are immiscible,[39] suggesting a significant role played by PEG proton-donating terminal hydroxyl groups in interaction with PVP. Fourier transform infrared spectroscopy studies have shown that miscibility in PVP–PEG blends containing various amounts of absorbed water is due to hydrogen bonding of hydroxyl groups at both ends of PEG short chains (see Fig. 1) to carbonyl groups in monomer units of PVP macromolecules.[40] Quantum chemical calculations have demonstrated that the most stable and energetically favorable network complexes arise when both PEG terminal OH-groups form H-bonds with PVP carbonyls, acting as comparatively long and flexible reversible noncovalent crosslinks between longer PVP macromolecules.[39] Molecules of absorbed water increase the gain in energy under PVP–PEG network complex formation from 33.7 to 79.4 kJ/mol.

Differential scanning calorimetry (DSC) studies of phase behavior of PVP–PEG–H_2O blends have been described in a series of publications.[41–43] In the first paper, interrelations among the temperatures of PEG melting, maximum cold crystallization rate, and PVP–PEG blend glass transition were examined.[41] Next, analysis of the PEG cold crystallization exotherm, coupled with the symmetric endotherm of PEG melting as functions of PVP–PEG blend composition and glass transition temperature, T_g, allowed us to evaluate the degree of PEG binding into network complex with PVP, because bound PEG is unavailable for cold crystallization and melting.[42] Lastly, the state of absorbed water in PVP–PEG blends was studied based on the analysis of the high-temperature endotherm of water thermodesorption. In particular, the amounts of absorbed water associated with PVP and PEG in their blends were evaluated.[43]

Extensive studies of the effect of PEG molecular weight on the phase behavior of PEG/PVP blends have been carried out.[44–46] Large negative deviations in measured T_g from the Fox equation were shown to be the result of hydrogen bond formation through the second terminal hydroxyl group of PEG short chains.[44] With this insight, the number of PEG chains crosslinking PVP macromolecules into a network complex was evaluated as a function of PVP–PEG blend composition. Nonequimolar stoichiometry of the PVP–PEG network complex was also established.[45] This phenomenon is due to a balance between the loss in entropy due to immobilization of PEG short chains in the course of their hydrogen bonding to PVP units through both chain ends, and the concomitant gain in entropy due to the increase in mobility of PVP chain segments between neighbor H-bonded junctions in the network complexes. The balance between these two entropic factors determines eventually the observed increase in PVP crosslinking degree with decrease in PEG molecular weight and defines the nonequimolar stoichiometry of formed H-bonded complexes.[45]

Finally, the phase behavior of PVP–PEG blends was examined over the entire composition range using temperature modulated differential scanning calorimetry (TM-DSC) and conventional DSC techniques.[46] Despite the unlimited solubility of PVP in oligomers of ethylene glycol, the PVP–PEG system under consideration demonstrated two distinct and mutually consistent relaxation transitions (heat capacity jumps), resembling glass transitions. The two observed T_gs were assigned to a coexisting PVP–PEG network (formed via multiple hydrogen bonding between PEG and PVP) and a homogeneous PVP–PEG blend (involving a single hydrogen bond formation per PEG molecule). Based on the established molecular details of self-organization in PVP–PEG solutions, a three-stage mechanism of PVP–PEG H-bonded complex formation/breakdown with increase of PEG content was proposed.[46]

Reversible network supramolecular structure of the self-assembled stoichiometric PVP–PEG H-bonded complex governs the rubber-like viscoelasticity[47,48] and relaxation properties of PVP–PEG blends.[49–51] Molecular dynamics in PVP–PEG–water blends was evaluated in terms of PEG, water, PVP, and PVP–PEG complex self-diffusion coefficients by pulsed field gradient NMR.[52,53]

By comparing experimental data on the structure and properties of the PVP–PEG model PSA, we are able to establish characteristics of polymer materials favoring pressure-sensitive adhesion. Part of this analysis was performed in our recent review.[33] Here we explore correlations between adhesive and mechanical properties on the one hand and the behavior of free volume in PVP–PEG blends; on the other hand, bridging the gap between nanostructure of the model PSA and its macroscopic physical properties. Although the model PVP–PEG adhesive demonstrates optimal adhesion at 36 wt % PEG-400 in blend and 6–12 wt % absorbed water, in the following discussion, we consider free volume, adhesion, and mechanical properties of the PVP blends with the PEG-400 over a wider range of compositions and absorbed water contents.

EXPERIMENTAL

Materials

PVP (M_w = 1,000,000 g/mol) and PEG (M_w = 400 g/mol) were obtained from BASF as Kollidon K-90 and Lutrol E-400, respectively. PEG fractions of molecular weights 200, 300, and 600 g/mol were purchased from Fluka. All polymers were used as received.

Sample preparation

For the peel test, adhesive films 250–300 μm in thickness were prepared by dissolving the PVP and PEG in ethyl alcohol and casting the solution on a 20-μm-thick poly(ethylene terephthalate) (PET) backing film. Films were dried for 3 days at ambient temperature (20–22°C), and then for 2 h under vacuum at 65°C. The dried adhesives were equilibrated with water at controlled vapor pressures at ambient temperature for 6–7 days. Equilibrium hydration of the PVP–PEG adhesive films ranged from 5% to 30%, consistent with water vapor sorption isotherms of PVP–PEG blends report earlier.[35]

For probe tack testing, 200-μm-thick adhesive films were prepared by casting solutions on microscope glass slides previously cleaned with ethyl alcohol. The films were dried first at room temperature during 24 h, then 2 h under vacuum, at 65°C. Water content in the adhesive films was then measured on a selected sample by weight loss after thoroughly drying in vacuum, 90°C. For all conditioned samples, the film contained 3 wt % water.

For measurements of tensile properties, unsupported 700-μm-thick adhesive films were produced by casting the solution onto a PEBAX-600 release liner (0.6-mm thick) and drying for 3 days at ambient temperature. Uniform thickness of the PVP–PEG films was provided using the BYK-Gardner film casting knife. After drying, the release liner was removed and unsupported PVP–PEG films were used for measurements.

Adhesion characterization

The adhesive joint strength of PVP–PEG blends was evaluated by 180° peel testing using an Instron 1221 tensile strength tester at peel rate 10 mm/min.[35] A low-density polyethylene (PE) film, 100 μm in thickness, crystallinity ~ 45%, and surface energy 28.5 mJ/m^2, was used as a standard substrate.

Probe tack testing was carried out at room temperature using a TA.XT.plus texture analyzer (Stable Micro Systems, UK) equipped with temperature/humidity control chamber. Compliance of the probe tack tester was 9.79 μm/N. A typical probe test involved three stages.[36] In the first stage, a flat stainless steel probe (diameter 4 mm) approached the adhesive layer lying on a microscope glass slide at a constant velocity of 2 mm/s. When the contact pressure reached 0.8 MPa, the probe stopped advancing and was held in position for 1 s. The probe was then removed at a constant debonding rate of 0.1 mm/s. The probe was cleaned with acetone after each test. Force versus time, $F(t)$, and displacement versus time, $d(t)$, curves were obtained from this test. Nominal stress (σ) and strain (ε) curves were obtained using the values of the initial film thickness (h_0) and the initial contact area (A_{Co}): $\sigma = F(t)/A_{Co}$ and $\varepsilon = (d(t) - h_0)/h_0$. Three to five probe tests were carried out at each condition. Stress–strain curves shown in this article are representative of one of these individual tests, whereas the mechanical parameters such as the practical work of adhesion (area under probe tack curve), the maximum stress σ_{max}, and the maximum extension ε_{max} are average values.

Mechanical testing

Tensile stress–strain behavior of the adhesive films was studied with an Instron 1222 Tensile Tester at ambient temperature. Dumbbell-shaped samples of the total length of 21 mm with a nip-to-nip distance of 10 mm were cut from rectangular films 0.5–0.7 mm in thickness. The width of the neck region was 5 mm. Tensile strength of the samples was determined at fixed cross head speed ranging from 10 to 100 mm per min, with 10 N full scale

load. The nominal (engineering) tensile stress, σ_N was defined as a stretching force normalized by the original cross-sectional area of the sample. Assuming uniform, constant volume deformation of the adhesive film along the neck region, the true tensile stress, σ_T, was calculated according to $\sigma_T = \sigma_N (1 + \varepsilon)$. Ultimate tensile strength and elongation at break were recorded. All reported stress–strain curves were reproduced in replicate experiments, varying less than 10%. The stress–strain curves were plotted in terms of nominal tensile stress, whereas the ultimate tensile stress, presented below, is true values.

Quantum chemical calculations

The contour length of PEG chains was predicted, taking into account the valence angles between covalent bonds linking the atoms of the polymer backbone, with complete optimization of geometric parameters by energy minimization, using Chem Office 2004 and the MOPAK, DFT, and GAUSSIAN programs.[54]

Nonequimolar stoichiometry of PVP–PEG complex

Stoichiometry was evaluated using an earlier described approach[44–46] based on the composition dependence of the negative deviations in glass transition temperature, T_g, from weight-average values, predicted by the simple rule of polymer mixing, i.e., the Fox equation.[55] According to this approach, the average number of PVP units between neighboring H-bonded PVP junctions is given by[46]

$$\frac{w_{\mathrm{PVP}} \cdot \mathrm{MW}_{\mathrm{PEG}}}{\mathrm{MW}_{\mathrm{PVP}} \cdot 2w^*_{\mathrm{PEG}}} \tag{1}$$

where $\mathrm{MW}_{\mathrm{PEG}}$ is the PEG molecular weight (200–600 g/mol), $\mathrm{MW}_{\mathrm{PVP}}$ is the molecular weight of PVP monomer unit, w^*_{PEG} is an adjustable parameter that is introduced into a modified Fox equation to fit DSC measurements of T_g dependence on the composition of PVP–PEG hydrated blends[44,46]:

$$\frac{1}{T_g} = \frac{w_{\mathrm{PVP}}}{T_{g\mathrm{PVP}}} + \frac{w_{\mathrm{H_2O}}}{T_{g\mathrm{H_2O}}} + \frac{w_{\mathrm{PEG}} + w^*_{\mathrm{PEG}}}{T_{g\mathrm{PEG}}} \tag{2}$$

where the w refer to the weight fractions. Because no negative deviations result from the formation of single hydrogen bond between one terminal hydroxyl in PEG molecule and PVP carbonyl,[44] w^*_{PEG} defines the weight fraction of PEG chains crosslinking the repeat units in PVP chains by means of two H-bonds.[45,46]

TABLE I
The compositions and degrees of hydration of PVP–PEG Blends Prepared Under Different Values of Relative Humidity for PALS Testing

No.	PVP–PFG composition (wt %)	Absorbed water (wt %)		
		RH = 10%	RH = 30%	RH = 50%
1	100 : 1	3.20	9.68	13.19
2	78 : 22	2.06	6.98	13.50
3	72.7 : 27.3	2.44	6.37	7.06
4	64 : 36	1.67	7.06	13.12
5	54.2 : 45.8	1.19	6.37	12.43

Free volume measurements

PALS[56] was used to assess the number density and size distributions of free-volume holes in PVP–PEG blends as a function of blend composition and RH. Compositions PVP–PEG–H_2O mixtures tested are listed in Table I.

For PALS measurements, the polymer films were prepared by dissolving the mixture or polymers in ethanol followed by casting the solution onto aluminum plates and drying for 2 days at ambient temperature (20–22°C). Films were subsequently dried for 7 days under vacuum at 28°C. The thickness of the coating was determined to be $\sim$ 200 μm using a profilometer (Alpha Step 200, Tencor, San Jose, CA).

PALS experiments were performed using positron sources both by a ^{22}Na radioisotope and by a variable mono-energy 30 keV positron beam at UMKC[34] for the bulk and depth profile free-volume properties, respectively. Each PAL spectrum contained 2 million counts. PAL data were fitted into four lifetime bins using the PATFIT program and also into continuous lifetime distributions using three programs: CONTIN, LT, and MELT. The three programs provided similar results, so we only present the smoothed lifetime distributions from MELT analysis.

RESULTS AND DISCUSSION

PVP–PEG blend as a nanostructured material

PVP and PEG each contain only one electron donating functional group in their repetitive units, and it is of no surprise that they are immiscible if PEG has a molecular weight of 1000 g/mol or higher.[39] However, PVP is readily soluble in liquid, lower molecular weight fractions of PEG, owing to hydrogen bonding of both PEG terminal OH-groups to carbonyl oxygen's in PVP.[37,40] Because any PEG short chain bears two terminal reactive hydroxyl groups, the formed H-bonded PVP–PEG complex has a network supramolecular structure, illustrated schematically in Figure 2.

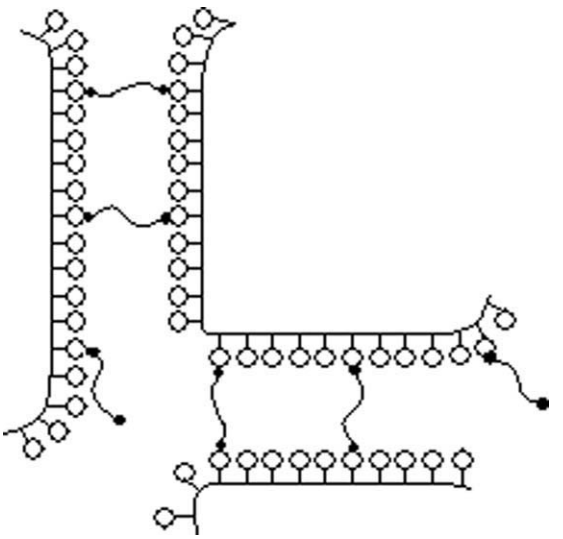

Figure 2 Schematic presentation of supramolecular structure of stoichiometric PVP–PEG network complex.

PEG chain length is a factor controlling the nonequimolar stoichiometry of PVP–PEG network complexes. Like an individual chemical compound, the stoichiometric PVP–PEG complex has been shown to demonstrate a composition invariant with the concentration of parent components in blend.[45] Hydrogen bonding of PEG terminal hydroxyls to the PVP carbonyls leads to a gain in enthalpy as a result of complex formation and loss in entropy due reduced conformational and translational freedom of the PEG chains. Unblended PVP is in a glassy state and its segmental mobility is essentially frozen. As illustrated in Figure 2, telechelic PEG chains act as spacers between PVP chains that increase the free volume and molecular mobility of PVP segments between neighboring H-bond network junctions. The longer the crosslinking PEG chains, the greater is the loss in entropy due to fixation of conformation and limitation of PEG chain translational mobility. To enable PVP–PEG network complex formation, a compensating mechanism is needed, counterbalancing the loss in entropy of PEG crosslinks. This mechanism can be provided by the increase in molecular mobility of PVP chain segments between two neighboring H-bonded network junctions. The longer the crosslinking PEG chains, the longer are the mobile PVP chain segments, and the sparser is the H-bonded network. When the entire PVP chain has already achieved sufficient mobility in the meshes of flexible H-bonded PVP–PEG network (Fig. 2), the compensating mechanism does not exist any longer and the network PVP–PEG complex has achieved its nonequimolar stoichiometry. In this way, the entropy loss compensating mechanism governs noncooperative mechanism of polymer–oligomer network complex formation.[57]

Dissolution of glassy PVP in liquid PEG is a two-stage process.[46] As PVP mixes with comparatively small amounts of PEG, a network complex forms. After the network complex has formed, OH-groups of excess PEG interact with PVP carbonyls through single terminal hydroxyl group, leaving the opposite terminal OH-group free of H-bonding with PVP. This second stage of PVP dissolution in PEG represents swelling of the network complex in excess PEG. Maximum adhesion is observed at the border between network complex formation and swelling.[33]

Figure 3 illustrates the effects of PEG molecular weight and chain length on the content of PVP units, crosslinked by H-bonding through both terminal PEG OH-groups, and the length of PVP chain segment between neighbor crosslinks, as calculated using eqs. (1) and (2). The fraction of crosslinked PVP units involved in stoichiometric complex is found to vary inversely with PEG molecular weight, providing insight into the nanostructured architecture of the stoichiometric PVP–PEG network complex. In PVP blends with PEG-400 and PEG-600, respectively, approximately every 5th and 10th PVP unit is involved in crosslinking through an H-bonded PEG chain. The average length of PVP chain segments between neighbor crosslinks is approximately half the length of crosslinking PEG chain. For PEG-400, the contour length PEG chain is 2.5 nm, whereas the length of PVP segment in the mesh of stoichiometric network complex is 1.23 nm. The most plausible explanation to this fact is that PVP is much stiffer than the PEG chain, which is appreciably bent due to its flexibility. In this connection, we can expect that the lengths of PVP chain segment and PEG crosslink in the mesh of H-bonded network are commensurable.

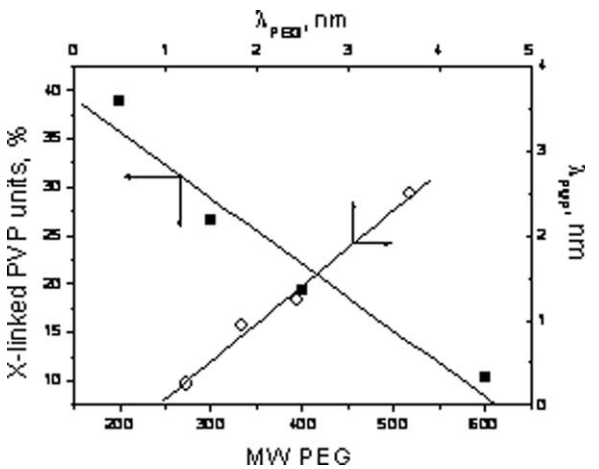

Figure 3 Content of PVP units (mol %), crosslinked by H-bonding through PEG chains in the blend [OH] : [PVP] = 1.132, and the length of PVP chain segments between neighbor crosslinks as the functions of PEG molecular weight and chain length.

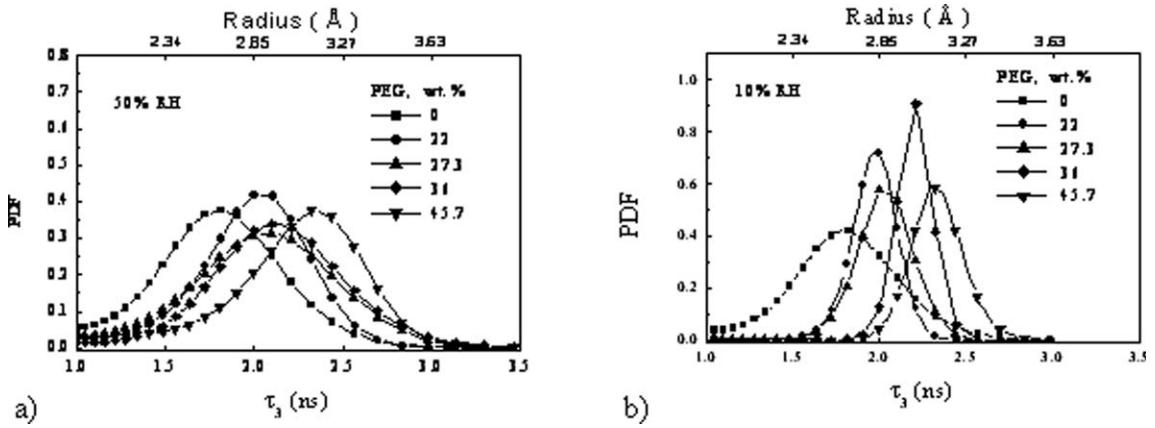

Figure 4 PDFs of *o*-Ps lifetime and distribution of free-volume holes in PVP–PEG blends of differing compositions at (a) RH = 50% and (b) RH = 10%. Lines are drawn to guide the eye.

PALS results

An energetic positron from a radioactive source entering a condensed medium thermalizes, losing its energy in a very short time, and then it annihilates with electrons of the medium.[58] The high sensitivity of PALS in probing defect properties arises from preferential trapping and localization of positronium (Ps, an "atom" consisting of a positron and an electron) in atomic-scale free volumes and holes. Because of the relatively small size of positronium (1.59 Å) and the short probe lifetime (~ nanoseconds), PALS is sensitive to small holes and free-volume defects in a size range of 1–20 Å and times of molecular motion from 10^{-10} s and longer.[58,59]

Positron lifetimes (τ_1, τ_2, and τ_3) and intensities (I_1, I_2, and I_3) from PAL spectra are attributed to *para*-positronium (*p*-Ps), positron (P), and *ortho*-positronium (*o*-Ps), respectively. The *o*-Ps lifetime τ_3, which is of order 1–5 ns in polymeric materials, is attributed to "pickoff" annihilation with electrons in molecules and is used to calculate the distribution of free-volume radius, *R* (Å to nm), based on an established semi-empirical correlation equation[60–62] for a spherical-cavity model, and to estimate the relative free-volume fractions.[58]

Probability density functions (PDFs) for *o*-Ps lifetimes and free-volume radius distributions for different PVP–PEG blend compositions and RH of surrounding atmosphere are shown in Figures 4 and 5. These figures indicate that mixing glassy PVP with liquid PEG-400 (plasticization) results in a shift of of τ_3, and hence, free-volume radius distribution toward higher values. The shift of distribution maximum toward longer τ_3 values is especially pronounced as the RH increases from 30% to 50%. Drying causes a downward shift in the distributions. The distribution profiles for PVP blends containing comparatively small amounts of both plasticizers (PEG-400 and water) are mostly symmetric, whereas those for the blends with high contents of PEG-400 and water are somewhat skewed to the left.

Effects of PVP–PEG composition and relative humidity on free-volume size and content

Figure 6(a,b) illustrate the effect of PVP–PEG blend composition on relative free-volume fraction and mean free-volume radius, respectively, at three different values of RH. Increasing PEG content from 0% to 43%, free-volume fraction increases by about 40%, whereas the mean hole radius increases by about 15%. Combining these observations and noting that volume scales as radius cubed, we infer that increased PEG content leads to a reduction in number density of free-volume holes in the blend.

It is also apparent from Figure 6(a,b) that RH has a greater effect on free-volume fraction than free-

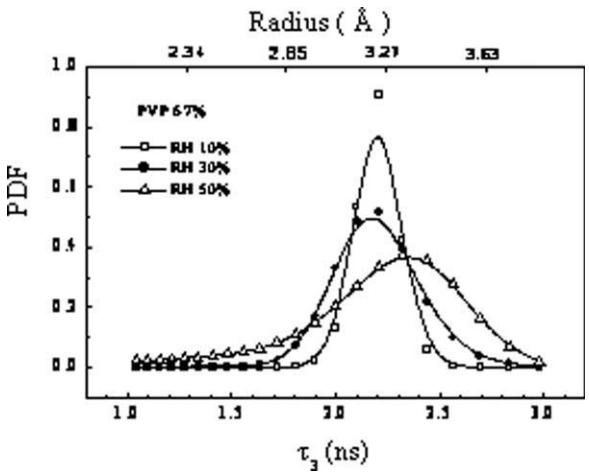

Figure 5 PDFs of *o*-Ps lifetime and distribution of the free-volume radius in PVP–PEG blend containing 33 wt % of PEG-400 for RH = 10%, 30%, and 50%. Lines are to guide the eye.

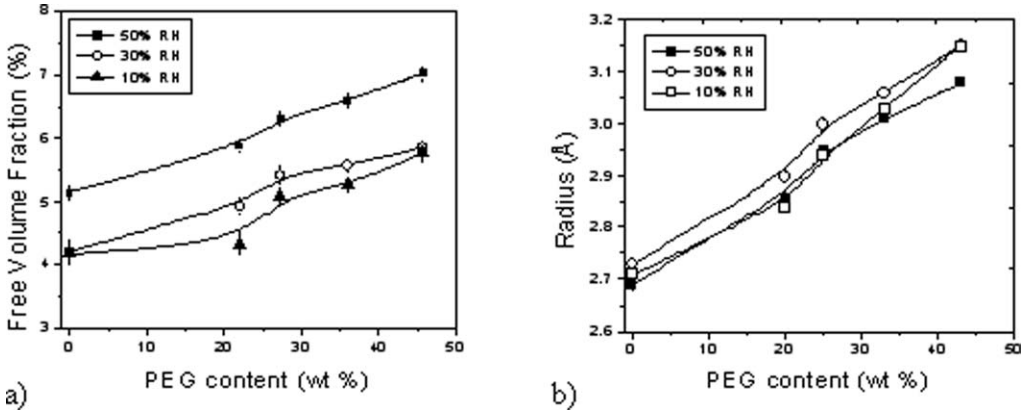

Figure 6 Free-volume statistics for PVP–PEG blend compositions at RH 10%, 30%, and 50%. (a) Relative free-volume fraction. (b) Mean free-volume radius.

volume radius. In Figure 7, the data in Figure 6 is replotted with RH as the abscissa. A direct correlation of RH with free-volume fraction is presented in Figure 7(a). The most pronounced increase in free-volume fraction occurs at RH change from 30% to 50%. Figure 7(b) confirms that RH has a negligible effect on free-volume radius. From Figures 6 and 7, it may be concluded that the effect of PVP–PEG blend composition on the free volume is much greater than that of RH.

Both PEG and absorbed water are good plasticizers of glassy PVP.[41–43] However, their plasticization mechanisms are appreciably different. Although increasing absorbed water concentration results in decreasing PVP–PEG blend T_g and cohesive strength, increase in PEG-400 concentration leads to an abnormally sharp decline of T_g and growth of cohesive strength, which is followed by the decrease of tensile strength as PEG content in blends exceeds the stoichiometric composition of the PVP–PEG network complex.[47] In this way, PEG behaves both as PVP plasticizer and a noncovalent crosslinker. This distinction between PEG and absorbed water behaviors is reflected also in their effects on the free-volume fraction and size, as shown in Figures 6 and 7. Although increase in PEG content causes the increase of both relative free-volume fraction and radius, absorbed water does not affect free-volume size, but increases the number density of free-volume holes.

Dispersion trends of free-volume radii are summarized in Figure 8. In dry blends (RH = 10%), the distribution of free-volume radii becomes narrower with increasing PEG content. At higher humidities, (30% and 50% RH), degree of dispersion passes through a maximum between 25% and 33% PEG concentration. The most hydrated blends (RH = 50%) exhibit significantly broader distributions of free-volume radius.

Figure 9 recasts the data of Figure 6 to demonstrate the relationship between mean volume of holes (cubic free-volume radius) and free-volume fraction in PVP–PEG blends of various hydration degrees. The relative free-volume fraction rises linearly with the cube of hole radius, indicating that no structural rearrangements occur in the blends. Actually, such rearrangements of supramolecular structure may affect the free-volume fraction even in

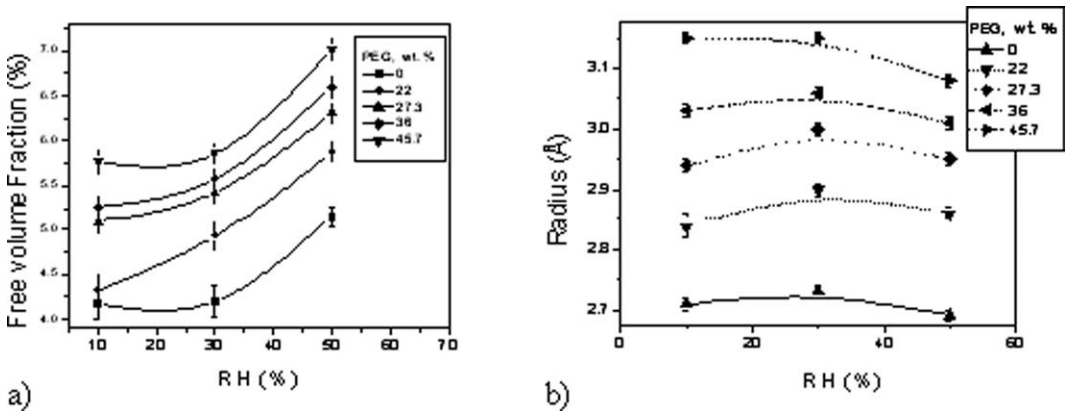

Figure 7 Effects of relative humidity on (a) free-volume fraction and (b) average free-volume radius in PVP blends with PEG-400.

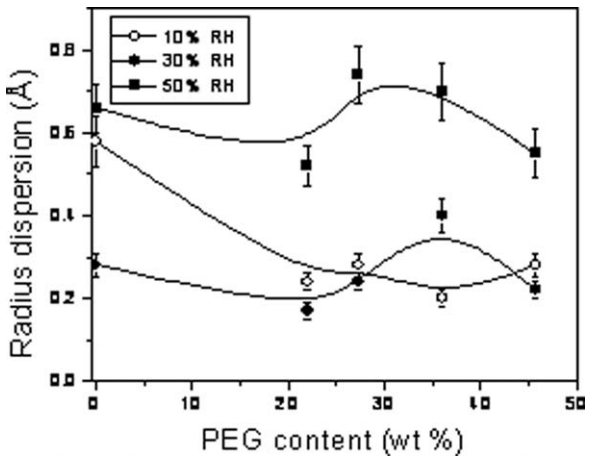

Figure 8 Effects of PVP–PEG composition and relative humidity on dispersion of free-volume radius.

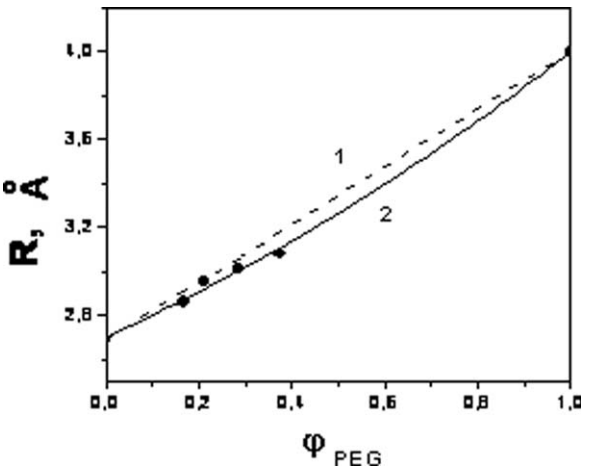

Figure 10 Relationship between PEG-400 volume fraction in the blends with PVP and average radius of free volume: 1, as calculated from the rule of additivity,[64] and 2, measured data.

the lack of the increase in the hole volume. Absorbed water has an insignificant effect on the slope of lines presented in Figure 9.

Structural rearrangements may occur only in dry PVP–PEG blends (RH = 10%), whereas a point corresponding to large free-volume radius deviates from the linear relationship, as shown in Figure 9. The slopes of the lines shown in Figure 9 are appreciably greater than unity, implying that the growth of relevant free-volume fraction under the increase of PEG concentration is due to the increase of both free-volume size and the amount of holes. The fact that the plots for comparatively dry blends (RH = 10% and 30%) practically coincide with each other is likely a result of tight association of small amounts of absorbed water with most hygroscopic component of polymer blends, PVP, in the first hydrate shell.[43,63]

As follows from the data shown in Figure 10, the relationship between free-volume radius and PEG content in the blends demonstrates small negative deviations from the weight-average values calculated in accordance with the rule of volume additivity. Such deviations can be explained by the contribution of hydrogen bonding between functional groups in PVP repeat units and terminal PEG groups, leading to the free-volume contraction.

Depth profile of *o*-Ps lifetime and free-volume radius

Adhesive bond formation is an interfacial phenomenon, so the profile of free-volume radius is of high importance. The existence of excess free volume at polymer interfaces is well recognized in literature.[65–71] Excess free volume facilitates interfacial PSA spreading and wetting of adherent surfaces under bonding pressure. In turn, interfacial excess

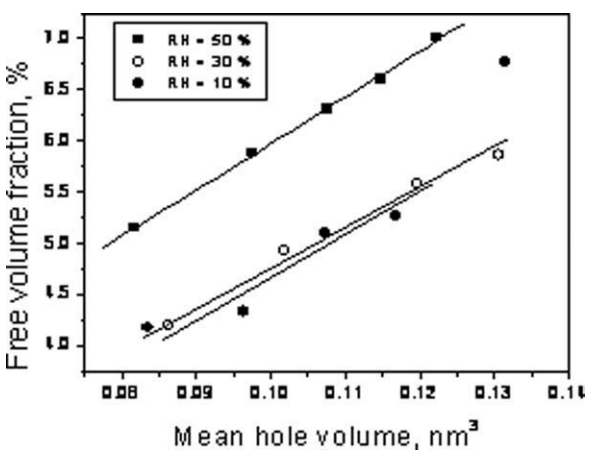

Figure 9 Relationship between average volume of holes [or cubic free-volume radius (nm^3)] and the relative free-volume fraction in the PVP–PEG blends of different compositions at 10%, 30%, and 50% RH.

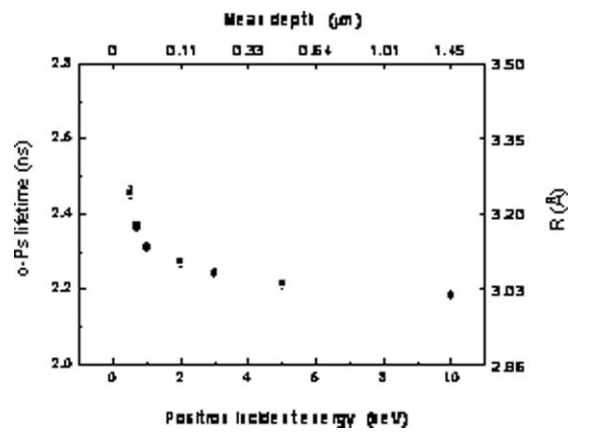

Figure 11 The *o*-Ps lifetime (τ_3 and hole size radius versus positron incident energy or depth from the film surface in PVP–PEG blend. Line was fitted to a model of layered structure of different values using VEPFIT.[34]

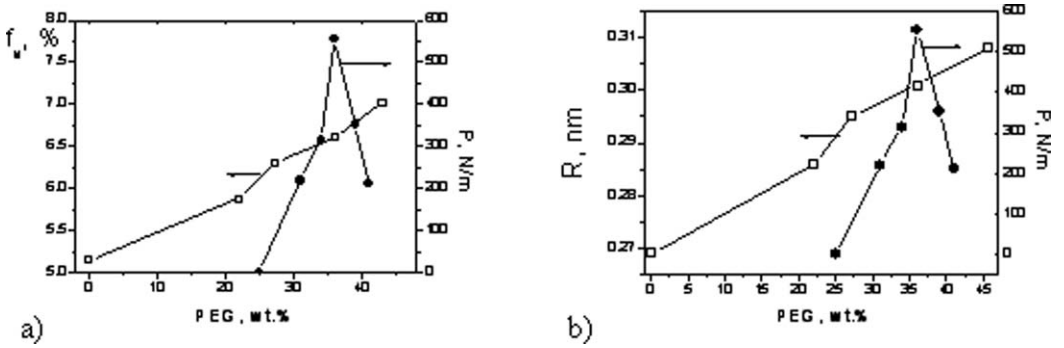

Figure 12 Effects of PEG content on peel adhesion (P) and free volume of PVP–PEG model PSA at RH = 50%. (a) Free volume fraction; (b) Average free volume radius.

free volume can result from the surface enrichment-depletion duality of polymer components in a binary polymer blend.[72–74]

As seen from Figure 11, *o*-Ps lifetime is longer close to the surface of the PVP–PEG blend, indicating the presence of larger free-volume holes near the surface. The lifetime distribution is also broader at the lower incident energies, suggesting a looser and wider range of packing of polymer chains at the surface than in the bulk of PSA polymer blend.

Excess interfacial free volume promotes rapid establishment of adhesive contact when slight bonding pressure is applied to PSA film. At the same time, the reduced free volume in the bulk of the PVP–PEG blend ensures dissipation of mechanical energy during debonding, as a detaching force is applied to the adhesive film. As has been shown, surface segregation in binary polymer mixtures usually leads to interfacial enrichment of the minor component.[73] In our case, the minor component is PEG oligomer. Thus, based on the data shown in Figure 7, we can suppose that the excess interfacial free volume is due to increased PEG-400 concentration on the surface of PVP–PEG adhesive film.

With the free-volume behavior in model PVP–PEG PSAs properly characterized, we can answer key questions: What values of free volume are responsible for high adhesion in the PVP–PEG blends? How does free volume relate to the viscoelastic properties of PVP–PEG model PSAs? Answers to these questions are of fundamental significance because they establish direct correlations between nanoscopic and macroscopic properties of PSA material.

Comparison of free volume and peel adhesion behaviors

Free-volume fraction and average free-volume radius and free-volume fraction along with peel adhesion force, are plotted versus PVP–PEG composition in Figure 12(a,b), respectively. Strongest adhesion is observed at free-volume content 6.3–7.0%, and free-volume radius varying between 2.95 and 3.08 Å.

Free volume and probe tack adhesion of PVP–PEG model PSA

The probe tack test is an illustrative and informative tool for characterizing adhesive joint strength, and for gaining qualitative insight into relative contributions of solid-like and liquid-like debonding mechanisms. The probe tack test imitates the process of touching the surface of a PSA film with a finger and sensing the force required to detach it. Probe tack stress–strain curves of PVP blends with various contents of PEG-400 are shown in Figure 13.

The strength of adhesive joints is evaluated in terms of maximum debonding stress or probe tack, σ_{max}, and the amount of mechanical energy dissipated during the debonding process, which is known as practical work of adhesion (W) and is measured as the area under stress–strain curve. It has been shown[75,76] that σ_{max} is a poorly reproducible quantity, whereas W is an accurate measure of adhesive strength. Values of these parameters are

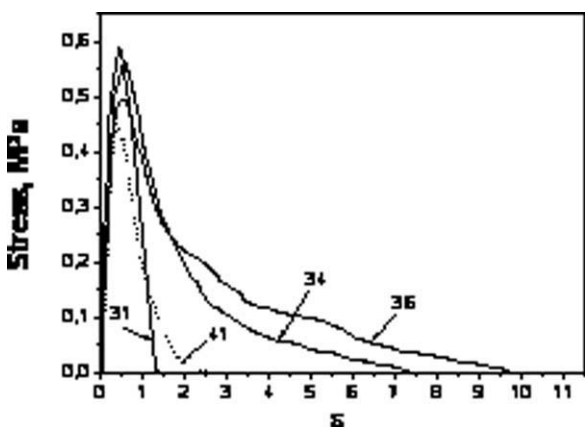

Figure 13 Probe tack curves of PVP blends containing different amounts (wt %) of PEG-400 and 3 wt % absorbed water.

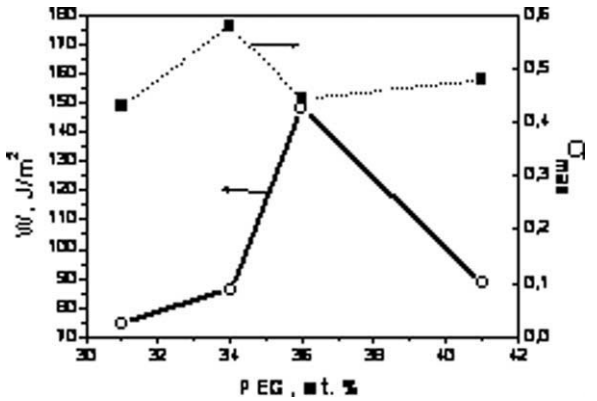

Figure 14 Practical work of adhesion, W, and the maximum debonding stress, σ_{max}, as functions of composition of PVP–PEG blends containing 3 wt % absorbed water.

plotted in Figure 14 as functions of PVP–PEG blend composition.

As is seen from the data presented in Figures 12 and 14, maximum peel and probe tack adhesion occurs with 36 wt % PEG-400. The data from the two tests do not necessarily coincide, because mechanisms of PSA deformation in the course of the tests are appreciably different. Although the contribution of shear strain to 180° peel adhesion is negligible,[77] which is not the case for probe tack debonding.

Probe tack curves provide detailed information on the mechanisms of PSA deformation and on debonding type. When the debonding curve has a symmetric peak with abrupt approach to zero stress, as observed for PVP blend with 31 wt % PEG-400 (Fig. 13), the PSA behaves as a solid-like material. In this case, the cohesive strength is higher than the strength of adhesive–substrate interaction, and the locus of failure is at the adhesive interface. If the peak of debonding stress is followed by the appearance of plateau or smooth stress reduction, as seen for PVP blends with greater amounts of PEG-400, failure is both adhesive and cohesive, and the PSA combines the properties of solid-like (great cohesive strength) and liquid-like materials (high fluidity).

A qualitative measure of PSA fluidity in probe tack curves is the maximum stretching of PSA layer, ε_{max}, at adhesive–substrate separation (debonding). The behavior of ε_{max} versus PVP–PEG blend composition is shown in Figure 15 along with the behaviors of free-volume fraction and radius for blends of comparable hydration (RH = 10%). No obvious correlation exists between ε_{max} and the free-volume parameters. However, it is pertinent to recall that, in PSAs, the transition point from a predominantly adhesive to a predominantly cohesive mechanism of debonding occurs at the point of maximum adhesion. Although free volume is a bulk property of polymer materials, adhesion is an interfacial phenomenon, including the contribution of adhesive–substrate interaction forces, which compete with PSA cohesive strength. Thus, although cohesive strength of PVP–PEG PSA dominates the strength of PSA-substrate interaction (PVP blends with 31%, 34%, and 36% PEG-400), both f_v and ε_{max} grow linearly with increasing PEG content (Fig. 15). As soon as the strength of interfacial forces becomes stronger than PSA cohesive strength, ε_{max} falls.

Relation of free volume to tensile properties of PVP–PEG model PSA

Both free volume and tensile strain are properties of bulk materials. It is, therefore, reasonable to search for correlations between free volume and mechanical properties such as tensile strain during uniaxial drawing of PVP–PEG blends. Figure 16 illustrates the effect of PEG-400 content on tensile stress–strain curves of the PVP–PEG blends. Values of maximum elongation at break, ε_b, and free-volume fraction are increasing linear functions of PEG concentration, as shown in Figure 16(b), suggesting that nanoscopic free volume, which governs molecular mobility of the PSA material, is a key factor underlying deformability of PVP–PEG blends.

It is noteworthy that both the size and the amount of free-volume voids have been reported to depend on polymer strain.[78,79] For polytetrafluoroethylene[78] in the region of elastic tensile deformation (ε = 0–20%), the hole concentration was shown to be nearly constant, with size slightly increasing with ε. At the end of the elastic stage, the larger stresses induced separation of polymer segments and formation of new free-volume holes, and free-volume fraction increased. In the plastic flow stage (ε = 20–80%), chain reorientation and polymer crystallization led to a decrease of free volume.[78] These results indicate that the linear correlation between the growth of

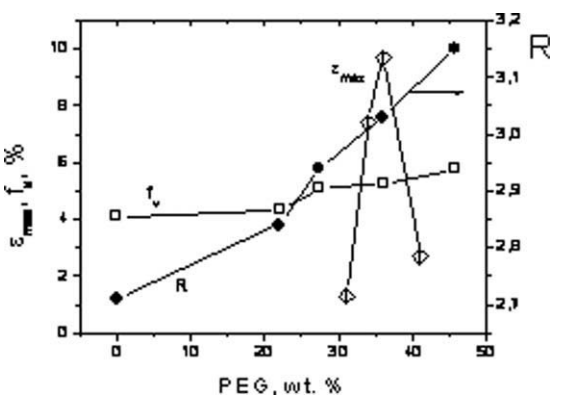

Figure 15 Maximum PSA stretch, ε_{max}, during probe tack test, relative free-volume fraction, f_v, and average free-volume radius, R (Å), as functions of composition of PVP–PEG blends.

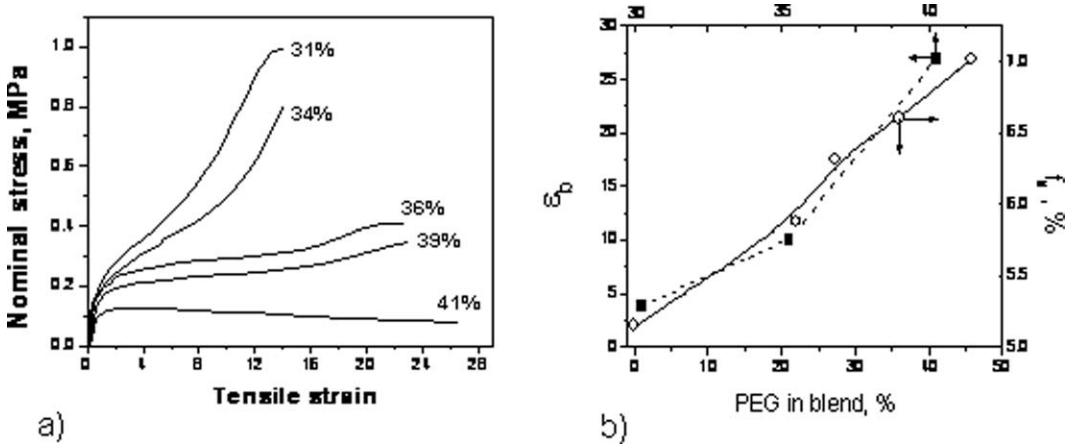

Figure 16 (a) Tensile stress–strain curves to break the PVP–PEG blends, containing 31, 34, 36, 39, and 41 wt % PEG-400. Content of absorbed water is 8–9 wt %. Drawing rate is 20 mm/min. (b) Effects of PEG content on maximum elongation at the break and free-volume fraction.

free volume and the value of maximum elongation, shown in Figure 16(b), applies only to viscoelastic amorphous polymers, which include all PSAs. In glassy polymers, tensile stress can lead to decrease of free volume.[80]

Figure 17 provides a summary of tensile and free-volume properties as a function of PEG composition. When comparing data presented in Figures 6 and 17, no direct correlations are seen between ultimate tensile stress, σ_b, the work of viscoelastic deformation until the break of PVP–PEG films, W_b, elastic tensile modulus, E, and the free-volume behavior. This finding is of no surprise, because all the latter tensile test characteristics include predominant contributions of cohesive strength. Thus, a unique feature of tensile testing is that it provides a feasible although indirect measurement of free volume, which is embodied in the maximum value of relative elongation at the break of adhesive film. This conclusion is especially valuable, because direct measurement of free volume requires the highly complex and expensive PALS technique. Qualitative estimation of free volume from maximum value of relative elongation based on tensile test data can be useful for comparative analysis of the structure and properties of viscoelastic polymers.

Tensile modulus of polymer materials (E) is defined as σ/ε ratio. The ratio σ_b/ε_b can be interpreted physically as an average modulus of the adhesive material before fracture. The quantity σ_b is an integral measure of cohesive strength of stretched polymer at the moment of polymer film break. In view of the linear relationship between relative free-volume fraction and maximum elongation of PVP–PEG PSA, shown in Figure 16(b), we can conclude that the σ_b/ε_b ratio or the break modulus of the stretched polymer defines at macroscopic level the fundamental ratio of cohesive strength to free volume, which governs not only pressure-sensitive adhesion but also mechanical properties of polymer materials.

Figure 18(a) illustrates the effect of hydration on tensile properties of the PVP/PEG networks. Reduced stress and increase elongation at break are consequences of increasing hydration. Figure 18(b) compares ε_b behavior with free-volume fraction and

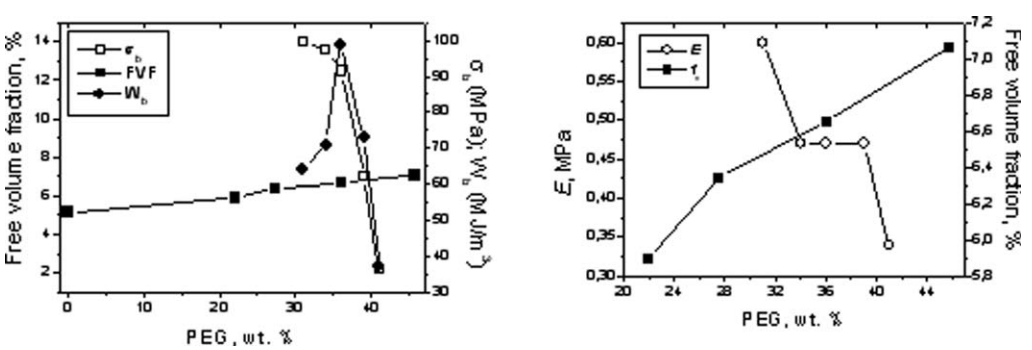

Figure 17 The total work of viscoelastic deformation to break the PVP–PEG film (W_b), the ultimate tensile strength (σ_b), elasticity modulus (E), and relative free-volume fraction (f_v), as the functions of PEG concentration in blends with PVP.

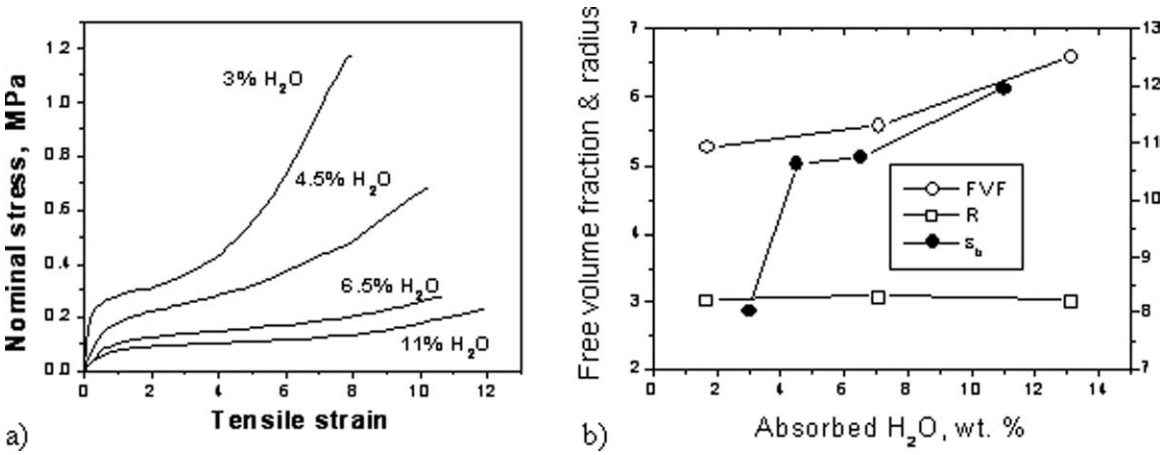

Figure 18 (a) Impact of absorbed water content in PVP/PEG blends with 36 wt % PEG-400 on tensile stress–strain curves under uniaxial drawing with at 20 mm/min. (b) Effect of absorbed water content (wt %) on tensile strain at break (ε_b), free-volume fraction (FVF, %), and average radius of free-volume holes (R, Å). Concentrations of absorbed water, corresponding to RH = 10%, 30%, and 50%, are taken from the data presented in Table I.

average radius of free-volume cavities. Mixing PVP with both plasticizers, PEG-400 and water, results in an increase in elongation at break. However, with the increase in PEG concentration, the value of ε_b increases linearly [Fig. 16(b)], whereas the same plot for the effect of water reveals a faster growth of ε_b in dry blends than in hydrated compositions [Fig. 18(b)]. Dry blends demonstrate also higher ultimate tensile stress values, implying that within the region of absorbed water contents between 3 and 4.5 wt %, cohesive strength contributes appreciably to deformability of polymer material, reducing the ε_b values. Subsequent growth of hydration degree leads to a gradual transition from brittle-like to rubber-like failure. On the basis of these results, we conclude that tracing the correlations between mechanical properties and free volume in polymer blends can be justified only for ductile, rubbery polymer materials that are capable to develop large tensile strains. For such polymers, the contribution of free volume to deformation mechanism dominates that of cohesive interaction energy.

As seen in Figure 18(b), above 4% concentration of absorbed water, linear growth of the ε_b correlates reasonably with linear increase of relative free-volume fraction, whereas no correlation is observed between the maximum tensile strain and the size of free-volume holes. This, combined with the observations surrounding Figure 7, suggest that the effect of free-volume fraction on mechanical properties of viscoelastic polymers is far greater than that of the size of free-volume holes. Because failure of adhesive joints involves mainly large strain mechanical behavior of viscoelastic PSA materials,[47,81,82] this conclusion may be also reasonably extended to the correlations between their adhesion and free-volume behaviors.

CONCLUSIONS

At the most fundamental molecular level, pressure-sensitive adhesion of polymer composites requires the combination of two generally conflicting properties: strong intermolecular cohesion and large free volume. In model PSAs based on blends of glassy high molecular weight PVP and liquid short-chain PEG, high-cohesive strength results from hydrogen bonding of PEG terminal hydroxyl groups to the carbonyls in pyrrolidone rings of PVP repeat units. Because every PEG molecule bears two terminal hydroxyls, the complex has a supramolecular network structure, wherein PEG chains play the role of reversible noncovalent crosslinkers and spacers between longer PVP macromolecules. Thus, the large free volume in PVP–PEG blends is due to appreciable length and flexibility of PEG chains. The length of PEG chains governs nonequimolar stoichiometry and nanometer size of the meshes of the H-bonded network. For example, if the contour length of PEG-400 chain is about 2.5 nm, the length of the PVP chain segment between neighbor crosslinks is approximately twice shorter.

Both PEG-400 and absorbed water are good PVP plasticizers. Nevertheless, as the rise in PEG concentration increases both free-volume radius and fraction, absorbed water leads to the increase in number density of free-volume holes, having no effect on the size of free-volume cavities. The depth profile of free-volume radius in the PVP–PEG-400 PSA demonstrates excess free volume on the surface of adhesive film ($\sim$ 3.25 Å at a depth of (20 nm) in comparison with bulky PSA (3.08 Å at the depth of 1.4 μm and more). Excess free volume at the surface facilitates wetting by the PSA polymer under slight bonding pressure, as shear deformation dominates. On

the other hand, residual free volume in the bulk facilitates dissipation of mechanical energy under detaching force, during which the PSA polymer demonstrates large tensile strain and fibrillation.

As comparison of free volume and peel adhesion behaviors has shown, best adhesion in PVP–PEG PSA is observed when the free-volume radius varies between 2.95 and 3.08 Å, and free-volume content ranges from 6.3% to 7.0%. In probe tack curves, if the contribution of interfacial adhesive–substrate interaction dominates that of cohesive strength of PSA material, then the radius and the relative fraction of free volume govern the value of maximum elongation. Finally, in tensile stress–strain curves, the size and relative fraction of free volume relate linearly to the maximum elongation to break in the PSAs, whereas both ultimate tensile strength and elasticity modulus vary inversely with free volume, as these quantities are determined by cohesive strength. Free-volume fraction is more important than free-volume hole size in controlling the tensile and adhesive properties of PVP–PEG PSAs.

The present research bridges the gap between molecular structure at the nanoscopic level and macroscopic physical properties of PVP–PEG model PSAs. Are the conclusions made for PVP–PEG model PSA also valid for the PSAs of different chemical structures? Are the correlations established here between free volume, adhesive, and mechanical properties indicative of causal relations? To answer these questions, analogous measurements should be performed in other typical PSAs, e.g., acrylic, polyisobutylene, rubber, and triblock copolymer adhesives. If similar correlations are observed, then a strong argument for causality and mechanism can be established.

References

1. Wang, B.; Wang, Z. F.; Zhang, M.; Liu, W. H.; Wang, S. J. Macromolecules 2002, 35, 3993.
2. Ferry, J. D. Viscoelastic Properties of Polymers, 3rd ed.; Wiley: New York, 1980.
3. Simha, R. Macromolecules 1977, 10, 1025.
4. Askadskii, A. A. Physical Properties of Polymers: Prediction and Control; Gordon and Breach Publishers: Amsterdam, 1996.
5. Dlubek, J.; Bamford, D.; Rodriguez-Gonzales, A.; Bornemann, S.; Stejny, J.; Schade, B.; Alam, M. A.; Arnold, M. J Polym Sci Part B: Polym Phys 2002, 40, 434.
6. Kobayashi, Y.; Zheng, W.; Meyer, E. F.; McGervey, J. D.; Jamieson, A. M.; Simha, R. Macromolecules 1989, 22, 2302.
7. Yampolskii, Y. P.; Kamiya, Y.;Alentiev A. Y. J Appl Polym Sci 2000, 76, 1691.
8. Krištiak, J.; Krištiakova, K.; Šauša, O.; Bandžuch, P.; Bartoš, J. J Phys II Colloq, 1993, 3, 265.
9. Wãstlund, C.; Schmidt, M.; Schrantz, S.; Maurer, F. H. J Polym Eng Sci 1998, 38, 1286.
10. Kumar, H.; Ranganathaiah, C. J Compos Mater 2008, 17, 1787.
11. Abdullah, M. A. M.; Altaweel, H. B.; Ravikumar, C.; Ranganathaiah, C. Phys Status Solidi A 2009, 6, 2401.
12. Wang, C. I.; Wang, S. J. J Phys Condens Matter 1994, 6, 3593.
13. Kakizaki, M.; Hideshima, T. Jpn J Appl Phys 1998, 37, 900.
14. Struik, L. C. E. Physical Aging in Amorphous Polymers and Other Materials; Elsevier: Amsterdam, 1978.
15. Fujita, H.; Kishimoto, A. J Chem Phys 1961, 31, 393.
16. Fujita, H.; Kishimoto, A. Polymer J 1991, 23, 1499.
17. Vrentas, J. S.; Duda, J. L. J Polym Sci Polym Phys Ed 1977, 15, 403.
18. Vrentas, J. S.; Duda, J. L. J Polym Sci Polym Phys Ed 1977, 15, 417.
19. Vrentas, J. S.; Duda, J. L. J Polym Sci Polym Phys Ed 1977, 15, 4441.
20. Vrentas, J. S.; Vrentas, C. M. Macromolecules 1994, 27, 1179.
21. Vrentas, J. S.; Vrentas, C. M. J Appl Polym Sci 1999, 71, 1431.
22. Putta, S.; Nemat-Nasser, S. Mater Sci Eng 2001, 317, 70.
23. Finkelshtein, E. S.; Makovetskii, K. L.; Gringolts, M. I.; Rogan, Y. V.; Golenko, T. G.; Starannikova, I. E.; Yampolskii, Y. P.; Shantarovich, V. P.; Suzuki, T. Macromolecules 2006, 39, 7022.
24. Barton, A. F. M. Handbook of Solubility Parameters and Other Cohesion Parameters, 2nd ed.; CRC Press: Boca Raton, 1991.
25. Barton, A. F. M. Handbook of Polymer Liquid Interaction Parameters and Other Solubility Parameters; CRC Press: Boca Raton, 1990.
26. Kinloch, A. J. Adhesion and Adhesives: Science and Technology; Chapman and Hall: London, 1987.
27. Dillard, D.; Pocius, A. V., Eds. Adhesion Science and Engineering—1, The Mechanics of Adhesion; Elsevier: Amsterdam, 2002.
28. Chaudhury, M.; Pocius, A. V., Eds. Adhesion Science and Engineering—2, Surfaces, Chemistry and Applications; Elsevier: Amsterdam, 2002.
29. Raetzke, K.; Shaikh, M. Q.; Faupel, F.; Noeske, P.-L. M. Int J Adhes Adhes 2010, 30, 105.
30. Garton, A.; Haldankar, G.; McLean, P. D. J Adhes 1989, 29, 13.
31. Chiang, M. Y. M.; Fernandez-Garcia, M. J Appl Polym Sci 2003, 87, 1436.
32. Benedek, I.; Feldstein, M. M., Eds. Handbook of Pressure-Sensitive Adhesives and Products, Vol. 1: Fundamentals of Pressure-Sensitivity; Vol. 2: Technology of Pressure-Sensitive Adhesives and Products; Vol. 3: Applications of Pressure-Sensitive Products; CRC—Taylor & Francis: Boca Raton, 2009.
33. Feldstein, M. M. In Fundamentals of Pressure Sensitivity; Benedek, I., FeldsteinM. M., Eds.; CRC—Taylor & Francis: Boca Raton, 2009; Chapter 10, pp 10–1–10–43.
34. Li, Y.; Zhang, R.; Chen, H.; Zhang, J.; Suzuki, R.; Ohdaira, T.; Feldstein, M. M.; Jean, Y. C. Biomacromolecules 2003, 4, 1856.
35. Chalykh, A. A.; Chalykh, A. E.; Novikov, M. B.; Feldstein, M. M. J Adhes 2002, 78, 667.
36. Roos, A.; Creton, C.; Novikov, M. B.; Feldstein, M. M. J Polym Sci Part B: Polym Phys 2002, 40, 2395.
37. Feldstein, M. M. Polym Sci Ser A 2004, 46, 1265.
38. Bairamov, D. F.; Chalykh, A. E.; Feldstein, M. M.; Siegel, R. A.; Platé, N. A. J Appl Polym Sci 2002, 85, 1128.
39. Bairamov, D. F.; Chalykh, A. E.; Feldstein, M. M.; Siegel, R. A. Macromol Chem Phys 2002, 203, 2674.
40. Kireeva, P. E.; Shandryuk, G. A.; Kostina, J. V.; Bondarenko, G. N.; Singh, P.; Cleary, G. W.; Feldstein, M. M. J Appl Polym Sci 2007, 105, 3017.
41. Feldstein, M. M.; Shandryuk, G. A.; Kuptsov, S. A.; Platé, N. A. Polymer 2000, 41, 5327.
42. Feldstein, M. M.; Kuptsov, S. A.; Shandryuk, G. A. Polymer 2000, 41, 5339.
43. Feldstein, M. M.; Kuptsov, S. A.; Shandryuk, G. A.; Platé, N. A.; Chalykh, A. E. Polymer 2000, 41, 5349.
44. Feldstein, M. M.; Shandryuk, G. A.; Platé, N. A. Polymer 2001, 42, 971.
45. Feldstein, M. M.; Kuptsov, S. A.; Shandryuk, G. A.; Platé, N. A. Polymer 2001, 42, 981.

46. Feldstein, M. M.; Roos, A.; Chevallier, C.; Creton, C.; Dormidontova, E. D. Polymer 2003, 44, 1819.
47. Novikov, M. B.; Roos, A.; Creton, C.; Feldstein, M. M. Polymer 2003, 44, 3559.
48. Feldstein, M. M.; Kulichikhin, V. G.; Kotomin, S. V.; Borodulina, T. A.; Novikov, M. B.; Roos, A.; Creton, C. J Appl Polym Sci 2006, 100, 522.
49. Novikov, M. B.; Borodulina, T. A.; Kotomin, S. V.; Kulichikhin, V. G.; Feldstein, M. M. J Adhes 2005, 81, 77.
50. Feldstein, M. M. Polym Sci Ser A 2009, 51, 1341.
51. Feldstein, M. M.; Novikov, M. B.; Creton, C. In Fundamentals of Pressure Sensitivity; Benedek, I., Feldstein, M. M., Eds.; CRC—Taylor & Francis: Boca Raton, 2009; Chapter 11, pp 11–1–11–62.
52. Vartapetian, R. S.; Khozina, E. V.; Kärger, J.; Geschke, D.; Rittig, F.; Feldstein, M. M.; Chalykh, A. E. Colloid Polym Sci 2001, 279, 532.
53. Vartapetian, R. S.; Khozina, E. V.; Karger, J.; Geschke, D.; Rittig, F.; Feldstein, M. M.; Chalykh, A. E. Macromol Chem Phys 2001, 202, 2648.
54. Foresman, J. B.; Frisch, E. Exploring Chemistry with Electronic Structure Methods, 2nd ed.; Gaussian, Inc.: Pittsburgh, PA, 1996.
55. Fox, T. G. Bull Am Phys Soc 1956, 1, 123.
56. For example, seeJean, Y. C.; Mallon, P. E.; Schrader, D. C., Eds. Principles and Applications of Positron and Positronium Chemistry; World Scientific Publisher: Singapore, 2003.
57. Feldstein, M. M.; Kireeva, P. E.; Kiseleva, T. I.; Gdalin, B. E.; Novikov, M. B.; Anosova, Y. V.; Shandryuk, G. A.; Singh, P.; Cleary, G. W. Polym Sci Ser A 2009, 51, 799.
58. For example, Jean, Y. C. Microchem J 1990, 42, 72.
59. Jean, Y. C. Macromolecules 1996, 27, 5756.
60. Tao, S. J. J Chem Phys 1972, 56, 5499.
61. Eldrup, M.; Lightbody, D.; Sherwood, J. N. Chem Phys 1981, 63, 51.
62. Nakanishi, N.; Wang, S. J.; Jean, Y. C. In Positron Annihilation Studies of Fluids; Sharma, S. C., Ed.; World Scientific: Singapore, 1988; p 292.
63. Lebedeva, T. L.; Feldstein, M. M.; Kuptsov, S. A.; Platé, N. A. Polym Sci Ser A 2000, 42, 989.
64. Bardyshev, I. I., unpublished results.
65. Freed, K.; Dudowicz, J. Pure Appl Chem 1995, 67, 969.
66. Siangchaew, K.; Libera, M. Microsc Microanal 1997, 3, 530.
67. Forrest, J. A.; Dalnoki-Veress, K. J Polym Sci Part B: Polym Phys 2001, 39, 2664.
68. Sills, S.; Overney, R. M. J Chem Phys 2004, 120, 5334.
69. Zhang, J.; Chen, H.; Liu, Q.; Chakka, L.; Jean, Y. C. ACS Symp Ser 2006, 941, 91.
70. Kajiyama, T. Macromol Res 2007, 15, 109.
71. Tanaka, K.; Tateishi, Y.; Okada, Y.; Nagamuta, T. J Phys Chem B 2009, 113, 4571.
72. Klein, J. In Polymer Surfaces, Interfaces and Thin Films; Karim, A., Kumar, S., Eds.; World Scientific: Singapore, 2000; p 81.
73. Budkowski, A.; Rysz, J.; Scheffold, F.; Klein, J.; Bernasik, A.; Jedlinski, J. Vacuum 1999, 54, 273.
74. Budkowski, A.; Rysz, J.; Scheffold, F.; Klein, J. Europhys Lett 1998, 43, 404.
75. Chiche, A.; Dollhofer, J.; Creton, C. Eur Phys J 2005, E 17, 389.
76. Creton, C.; Shull, K. R. In Fundamentals of Pressure Sensitivity; Benedek, I., Feldstein, M. M., Eds.; CRC—Taylor & Francis: Boca Raton, 2009; Chapter 6, pp 6–1–11–26.
77. Kaelble, D. H. In Handbook of Pressure-Sensitive Adhesive Technology, 3rd ed.; Satas, D., Ed.; Satas & Associates: Warwick, Rhode Island, 1999; Chapter 6, pp 96–120.
78. Wang, S. J.; Wang, C. I.; Wang, B. J Phys IV Colloq 1993, 3, 275.
79. Mohsen, M.; Gomaa, E.; Sharaf, M. A.; Salem, H.; Gomaa, W. Int J Nano Biomater 2009, 2, 279.
80. Riggleman, R. A.; Lee, H.-N.; Ediger, M. D.; de Pablo, J. J. Phys Rev Lett 2007, 99, 215501.
81. Creton, C.; Hu, G.; Deplace, F.; Morgret, L.; Shull, K. R. Macromolecules 2009, 42, 7605.
82. Derail, C.; Marin, G. In Fundamentals of Pressure Sensitivity; Benedek, I., Feldstein, M. M., Eds.; CRC—Taylor & Francis: Boca Raton, 2009; Chapter 4, pp 4.1–4.26.